Bulletin of the Seismological Society of America, Vol. 96, No. 3, pp. 1140–1158, June 2006, doi: 10.1785/0120040239

Ⓔ

Fault Parameter Constraints Using Relocated Earthquakes: A Validation of First-Motion Focal-Mechanism Data

by Debi Kilb and Jeanne L. Hardebeck

Abstract We estimate the strike and dip of three California fault segments (Calaveras, Sargent, and a portion of the San Andreas near San Jaun Bautistia) based on principle component analysis of accurately located microearthquakes. We compare these fault orientations with two different first-motion focal mechanism catalogs: the Northern California Earthquake Data Center (NCEDC) catalog, calculated using the FPFIT algorithm (Reasenberg and Oppenheimer, 1985), and a catalog created using the HASH algorithm that tests mechanism stability relative to seismic velocity model variations and earthquake location (Hardebeck and Shearer, 2002). We assume any disagreement (misfit $>30^\circ$ in strike, dip, or rake) indicates inaccurate focal mechanisms in the catalogs. With this assumption, we can quantify the parameters that identify the most optimally constrained focal mechanisms. For the NCEDC/FPFIT catalogs, we find that the best quantitative discriminator of quality focal mechanisms is the station distribution ratio (STDR) parameter, an indicator of how the stations are distributed about the focal sphere. Requiring STDR > 0.65 increases the acceptable mechanisms from 34%–37% to 63%–68%. This suggests stations should be uniformly distributed surrounding, rather than aligning, known fault traces. For the HASH catalogs, the fault plane uncertainty (FPU) parameter is the best discriminator, increasing the percent of acceptable mechanisms from 63%–78% to 81%–83% when FPU $\leq 35^\circ$. The overall higher percentage of acceptable mechanisms and the usefulness of the formal uncertainty in identifying quality mechanisms validate the HASH approach of testing for mechanism stability.

Online material: 3D visualization of relocated earthquakes and accuracy of focal mechanisms.

Introduction

Accurate fault orientation parameters (strike and dip) play a key role in many geophysical studies (e.g., Gomberg and Ellis, 1994; Hsu and Sibuet, 1995; Carena and Suppe, 2002; Rundquist and Sobolev, 2002; Bilek *et al.*, 2003; Steacy *et al.*, 2005). Some fault orientation estimates are relatively straightforward to attain based on field mapping (e.g., Rockwell *et al.*, 2002) or on microearthquake delineation of fault planes (e.g., Rubin *et al.*, 1999; Waldhauser and Ellsworth, 2002). However, even in well-instrumented regions, fault strike inferred from standard network catalogs of microseismicity can be as much as 90° in error (e.g., Kilb and Rubin, 2002).

The quality of fault orientation parameters, such as those compiled in earthquake focal mechanism catalogs, is difficult to quantify because the true fault plane orientations are often unknown. One difficulty in determining fault orientations geologically is the limited number of locations where faults intersect deep boreholes. This forces us to rely on extrapolations of point measurements of fault orientations at depth to estimate the full geometry of the fault system. Combining information from independent datasets, such as aftershock locations, focal mechanism data, geomorphology, and geology (e.g., Hessami *et al.*, 2001; Segall, 2002), is the most effective method of constraining fault parameters. Yet, sometimes the results from different datasets can be in disagreement. For example, the expected mainshock fault orientation of the New Zealand 1994 Arthur's Pass M_w 6.7 earthquake has discrepancies among solutions from the Harvard Centroid Moment Tensor (CMT) (Dziewonski *et al.*, 1995), the aftershock distribution (Robinson *et al.*, 1995), the Global Positioning System (GPS) modeling results (Arnadottir *et al.*, 1995), and initial body-wave modeling results (Abercrombie *et al.*, 1996). Abercrombie *et al.* (2000) suggest these differences arise from a nonplanar mainshock fault. Assessing the accuracy of the data and the associated uncertainty estimates is critical in determining if the differ-

ences are explainable (e.g., Robinson *et al.*, 2001; Garcia *et al.*, 2002) and/or which takes precedence.

Earthquake focal mechanisms derived from binary up/down first-motion polarity data can be subject to errors caused by low signal-to-noise in the seismic waveform, complexity in the initial part of the waveform, instrumental polarity problems, 3D velocity variations, or simple human errors in identifying the first motion polarity (e.g., Oppenheimer *et al.*, 1988). Some of these erroneous signals or inaccuracies can be accounted for or removed. Yet, the extra effort to refine first-motion data is daunting, and many researchers opt not to question archived data from established data centers and instead take the cataloged uncertainty estimations at face value. Our aim is to determine the easiest and most efficient way to attain quality focal mechanisms using readily available data.

To help researchers discriminate between well- and poorly constrained solutions, many data centers provide catalogs of earthquake locations, magnitudes, and focal mechanisms that include uncertainty estimates in the strike and dip of the fault plane. For simplicity, sometimes users of these catalogs do not use the uncertainty estimates at all. Alternatively, a subset of the data that is expected to be "bad" (e.g., smaller magnitude earthquakes) is not used, or data with large formal uncertainties are eliminated. This thinning of the data is at times done without questioning the accuracy of the uncertainty estimates. We investigate how these choices can potentially bias research results.

Here, we introduce a methodology that others can use to determine how to obtain and generate quality focal mechanisms. Quality parameters that are known to discriminate between good- and poor-quality focal mechanisms, instead of those that "should" be a good discriminant, have the potential to greatly reduce uncertainties and improve research results. Such high-quality catalogs are important for a range of users and a range of purposes including (1) immediate use by users of FPFIT and HASH focal mechanism datasets, by aiding them in data selection; (2) intermediate use by those planning to compile and use new focal mechanism catalogs, by highlighting the pros and cons of the FPFIT and HASH methods; and (3) long-term use for science, because as the quality of mechanisms catalogs improves, the research based on these catalogs will also improve.

We use relocated data (created using cross-correlation methods) to help us infer the true fault structure, strike, and dip, of each of our study regions. The advantage of using cross correlation of seismic waveforms, which substantially reduces the uncertainties in relative earthquake locations, is that noisy data, usually discarded from first-motion studies, can often be used. These refined earthquake locations can be used to estimate fault strike and dip of both primary and secondary faults (e.g., Kilb and Rubin, 2002; Schaff *et al.*, 2002). In this way, the orientation of a rupture plane many kilometers long can be estimated to within $\pm 10°$, thus eliminating the inherent nodal plane ambiguity in the focal mechanism data.

In this study, we compare two focal mechanism catalogs, one generated with the computer program FPFIT (Reasenberg and Oppenheimer, 1985) and the other with the computer program HASH (Hardebeck and Shearer, 2002), with the orientation (strike, dip, and assumed right-lateral slip) of the corresponding faults delineated by relocated earthquakes. This allows us to assess the goodness of the cataloged focal mechanism parameters and the uncertainty estimates, and to identify which quality parameters (e.g., station distribution, azimuthal gap, fit quality factor, number of observations) best identify well-constrained focal mechanisms. Our overall goal is to identify the best discriminators, which can be used by future researchers, to easily select the highest-quality data. (Ⓔ See supplemental material in the electronic edition of BSSA.)

Data

We study three California fault segments: the Sargent fault, the Calaveras fault near the 1984 Morgan Hill M 6.2 earthquake, and the San Andreas fault (SAF) just south of the 1989 M 7.1 Loma Prieta earthquake (Fig. 1). For these regions, ~11,525 earthquakes are cataloged at the Northern California Earthquake Data Center (NCEDC) that were recorded between 1984 and 1997, and of these, 7555 events were relocated using the waveform cross-correlation technique of Got *et al.* (1994) (see the next section; note that Allan Rubin relocated the data in the Calaveras and SAF catalogs; see Rubin, 2002b). This subset of 7555 relocated earthquakes span depth ranges of approximately 2–10 km and earthquake magnitudes of 0.5–3.6. The median earthquake magnitude in the relocated datasets is 1.2, 1.4, and 1.1 for the Calaveras fault, SAF, and Sargent fault data, respectively, and each of these catalogs is complete to magnitude ~1.0. The majority of seismic stations in this study have been operational for many years, and problems such as reversed polarity and timing errors are well documented (e.g., Rubin, 2002a).

We use the results from two different algorithms that compute focal mechanisms: FPFIT (Reasenberg and Oppenheimer, 1985) and HASH (Hardebeck and Shearer, 2002). Both use a grid search to identify the mechanisms with the minimum misfit of the up/down first-motion polarities. The main difference in the methodologies of these programs is that HASH considers the stability of the solutions with respect to variations in earthquake location, seismic velocity model, and potential errors in the polarity measurements, whereas FPFIT finds the best solution assuming these quantities are exactly known.

We do not compute the FPFIT mechanisms ourselves; instead we use FPFIT results already cataloged in the NCEDC focal mechanism catalog (we refer to this catalog as NCEDC/FPFIT). Of the 7555 relocated earthquakes in our dataset, 3440 have cataloged focal mechanisms at the NCEDC. Discarding the 1219 mechanisms that have multiple solutions, or solutions that did not converge to an answer, our final

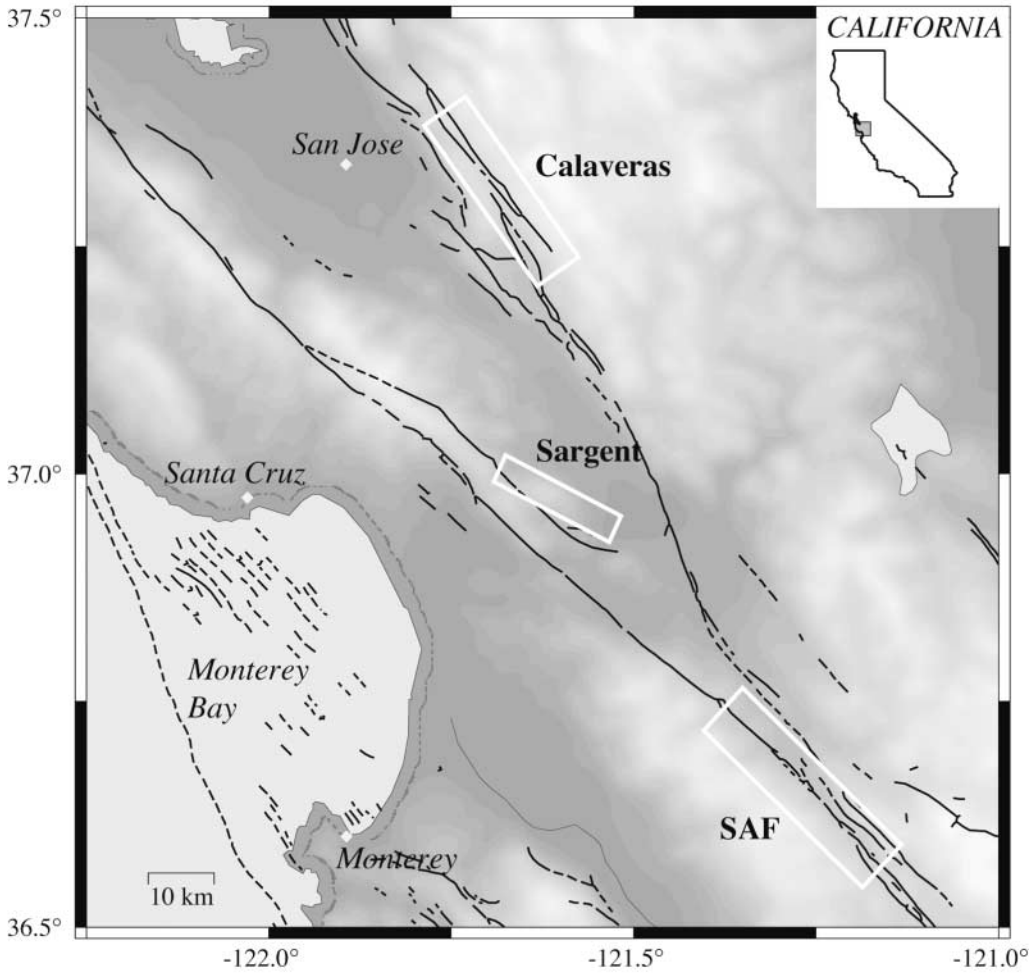

Figure 1. Study region in California (inset). Our three study areas (rectangles from top to bottom) include the Calaveras fault near the Morgan Hill *M* 6.2 1984 earthquake (Calaveras), the Sargent fault (Sargent), and the San Andreas fault (SAF). Solid and dashed lines represent known and inferred fault traces. For the Sargent fault data we chose the region encompassing the linear seismicity trend at depth, which does not align with the mapped surface trace.

NCEDC/FPFIT catalog is reduced to 2221 events (Table 1). This catalog also includes a number of mechanism quality parameters, which are automatically computed by the FPFIT program (Table 2).

The HASH catalog, which we generated, does not contain multiple solutions for an individual earthquake (otherwise the focal mechanism would have a reduced quality grade), and so no data is discarded from the HASH catalog. We did, however, require 4 or more polarity measurements for each mechanism. Earthquakes with fewer than 4 polarity measurements were not assigned a focal mechanism. The focal mechanisms with only 4 polarities are expected to be of poor quality; they are included so that we may constrain the minimum number of polarity observations that are necessary. In this way, we computed 5623 mechanisms for the same set of 7555 relocated earthquakes, and a number of mechanism quality parameters (Table 3). For consistency with the FPFIT dataset, we used the NCEDC catalog locations and first motions. The number of events common to both the NCEDC/FPFIT and HASH catalogs are 785, 1013, and 198 for the Calaveras, SAF, and Sargent datasets, respectively.

Table 1
The Number of Earthquakes in Each Data Subset, Which Varies from Differences in the Way the Computer Codes FPFIT and HASH Generate the Focal Mechanism Catalogs

Fault	No. of Relocated Earthquakes	No. Mechs. FPFIT*	No. Mechs. HASH†	Number of Common Events‡
Calaveras	3660	988	2809	785
San Andreas	3230	1025	2397	1013
Sargent	665	208	400	198
Total	7555	2221	5606	1996

*Relocated and converged solution and nonmultiple solution.
†Relocated.
‡Common to HASH and FPFIT catalogs; relocated.

Table 2
Parameters of Interest That are Computed with the FPFIT Program (Available in the NCEDC Catalog)

Parameter (acronym)	Values	Description
Number of observations (NOBS)	Data dependent	Number of observations used in the solution.
Station distribution ratio (STDR)	0.0–1.0	Sensitive to the distribution of the data on the focal sphere, relative to the radiation pattern. Low values (say, STDR < 0.5) indicate a relatively large numbers of the data points lie near nodal planes in the solution.
Error in strike (ΔSTR)	0°–180°	Uncertainty in the strike parameter (e.g., $\pm\Delta$STR).
Error in dip (ΔDIP)	0°–90°	Uncertainty in the dip parameter (e.g., $\pm\Delta$DIP).
Error in rake (ΔRAK)	0°–360°	Uncertainty in the rake parameter (e.g., $\pm\Delta$RAK).
Maximum Azimuthal Gap (AZGAP)	0°–360°	The maximum azimuthal angle between adjacent stations.
(No. machine picks)/ (No. of hand picks)	0–1	The percentage of automated seismic arrival picks versus analyst seismic arrival picks; 0 indicates all hand picks.
Fmin (MISFIT = 100∗Fmin)	0–1	Evaluation of overall fit; 0.0 represents a perfect fit to the data, while 1.0 represents a perfect misfit.
RMS travel-time residual	Data dependent	RMS of the travel time residual. Smaller values indicate a preferred solution.
Number of weights > 0.1 (NW)	Data dependent; an integer value	The number of *P* and *S* times with weights greater than 0.1.

For a more complete description see Reasenberg and Oppenheimer (1985).

Method

Cross Correlation of Seismic Waveforms

The relative locations of microearthquakes can be determined using cross correlation of similar seismic waveforms from nearby earthquake pairs (e.g., Got *et al.*, 1994; Waldhauser *et al.*, 1999; Waldhauser and Ellsworth 2000), and the accuracy of these relative positions typically surpasses the original catalog accuracy by an order of magnitude or more. In this way, small-scale fault complexity, on the order of tens of meters, is delineated by the relocated earthquakes (e.g., Rubin *et al.*, 1999; Rowe *et al.*, 2002; Shearer, 2002; Waldhauser and Ellsworth, 2002; Fukuyama *et al.*, 2003; Roumelioti *et al.*, 2003; Scarfi *et al.*, 2003). Here, the method of Got *et al.* (1994) is used to determine relative locations of subsets (multiplets: 14 for the Sargent fault, 34 for the Calaveras fault, and 57 for the SAF) that consist of 7–35 events in which the cross-correlation measurements use 2.56 sec (256 sample points) of *P*- and *S*-waveform data for each earthquake pair. The absolute location of each individual multiplet is determined from the centroid of the original catalog locations. The relative location errors between multiplets can be twice as large as the errors of their original catalog locations. We assume that such errors do not bias our results because these absolute location uncertainties (several hundreds of meters) can change the strike or dip of a fault plane ~10 km long by no more than 0.6°, which is substantially smaller than our assumed 30° uncertainty estimate (Fig. 2). Similarly, uncertainties in strike and dip that result from grouping the earthquakes in different multiplets is very small (<1°). In some cases the method used to relocate the data may influence the results (Wolfe, 2002; Michelini and Lomax, 2004), but for this study, where we are concerned with only the large-scale strike and dip orientation of the fault, the choice of relative relocation method is inconsequential (i.e., for this study, relocation methods HYPODD and Got *et al.*, [1994] would likely yield exactly the same general overall fault orientation results: compare Schaff *et al.*, [2002] with Rubin and Gillard [2000]).

Focal Mechanism Determination

Many methods can be used to compute focal mechanisms: using initial polarity of the *P* wave (e.g., Reasenberg and Oppenheimer, 1985) or the *P* and *S* waves (e.g., Nakamura, 2002); spectral amplitudes combined with *P*-wave polarities (e.g., Lund and Boovarsson, 2002); *S*/*P*-wave amplitude ratios (e.g., Kisslinger, 1980; Julian and Foulger, 1996; Hardebeck and Shearer, 2003); or inversion of full waveforms (e.g., Dreger and Helmberger, 1993; Fukuyama *et al.*, 2003). The method chosen typically depends on data availability and project goals.

First-motion focal mechanisms are frequently computed with the computer program FPFIT (Reasenberg and Oppenheimer, 1985), which can be obtained by anonymous FTP from http://quake.wr.usgs.gov/research/software/index.html#FP. This program requires as input the azimuth and angle of the seismic ray to each station as it leaves the seismic source and the first-motion polarity (up/down) of the *P* wave recorded at the station. The computer code HASH (Hardebeck and Shearer, 2002) is an improvement upon the FPFIT program because it takes into account the sensitivity of the focal mechanism to the computed takeoff angle from the hypocenter, the earthquake depth, and seismic velocity model (in this study we tested for velocity model sensitivity

Table 3
Focal Mechanism Quality Parameters That Are Computed by the HASH Program

Parameter (acronym)	Values	Description
Fault plane uncertainty (FPU)	0°–90°	1-sigma fault plane uncertainty, defined as RMS angular difference of the acceptable fault planes from the preferred plane.
Fmin (MISFIT = 100∗Fmin)	0–1	Evaluation of overall fit; 0.0 represents a perfect fit to the data, while 1.0 represents a perfect misfit.
Station distribution ratio (STDR)	0.0–1.0	Sensitive to the distribution of the data on the focal sphere, relative to the radiation pattern. Low values (say, STDR < 0.5), indicate a relatively large numbers of the data points lie near nodal planes in the solution.
Maximum azimuthal gap (AZGAP)	0°–360°	The maximum azimuthal angle between adjacent stations.
Number of first-motion observations (NOBS)	Data dependent	Number of phases used in the focal mechanism determination.
HASH quality factor (HASHQ)	A–F	A quality factor based on the robustness of the solution:

Quality (Q_HASH)	Average Misfit (Fmin)	RMS Fault Plane Uncert. (FPU)	Station Distribution Ratio (STDR)	Mechanism Prob. (PROB)
A	≤0.15	≤25°	≥0.5	≥0.8
B	≤0.20	≤35°	≥0.4	≥0.6
C	≤0.30	≤45°	≥0.3	≥0.7
D	Maximum azimuthal gap ≤90°, maximum takeoff angle gap ≤60°			
E	Maximum azimuthal gap >90°, maximum takeoff angle gap >60°			
F	Fewer than 8 polarities			

Mechanism probability (PROB)	0.0–1.0	Fraction of acceptable solutions close to preferred mechanism (relative probability of multiple solutions). Larger values are preferred.		

For a more complete description of HASH see Hardebeck and Shearer (2002).

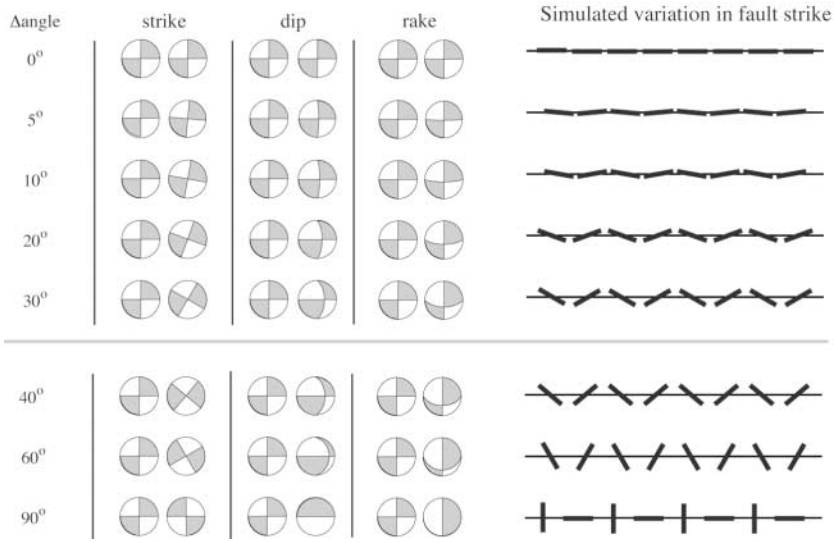

Figure 2. Qualitative examination of the variability in fault orientations and variability in focal mechanisms. We assume that two focal mechanisms are consistent with each other if their strike, dip, and rake differ by less than 30° (i.e., pairs above the horizontal line).

using the NCEDC 1D velocity models: coy, lew, lom, lon, mor, and ncg; for more information see http://quake.geo.berkeley.edu/ftp/pub/doc/cat5/ncsn.catalog.y2k.5) when computing solutions and error estimations. The HASH program can be obtained from http://quake.wr.usgs.gov/research/software/index.html#HASH. Using a grid search similar to that of FPFIT, HASH determines the focal mechanism quality based on the robustness of the solution with respect to variations in seismic velocity model, earthquake depth, and random polarity errors. The final HASH quality grade (HASH-Q) is based on the stability of the solution, quantified as the fault plane uncertainty (FPU), the fraction of misfit polarities, and the station distribution ratio (STDR). In this work we compare the FPFIT and HASH focal mechanism catalogs and pinpoint associated parameters that can be used to maximize the quality of the data.

Quantifying the Quality of Individual Earthquake Focal Mechanisms

For each of the three faults in this study, we estimate fault strike and dip using principal component analysis

Table 4
Fault Orientations Determined from Principle Component Analysis of the Relocated Earthquake Data (Figs. 1 and 3)

Fault	Number of Events	Strike	Dip	Assumed Rake
Calaveras	3660	N32°W	84°	180° (right lateral)
San Andreas	3230	N46°W	85°	180° (right lateral)
Sargent	665	N63°W	87°	180° (right lateral)

(MATLAB® routine PCACOV) of the relocated earthquakes. We do not attempt to include the unrelocated data, as we do not expect all earthquakes to precisely locate on one single fault. The extreme similarity in waveforms and the narrow band of seismicity delineated by the relocated events indicate that the 7555 relocated earthquakes in this study define the main faults rather than off-fault or cross-fault features. We therefore assume the fault plane of each earthquake in our relocated catalog aligns with the main strike and dip of these delineated faults. Of the two possible nodal planes in the focal mechanism catalogs, we choose the plane that is most consistent with the strike of the relocated seismicity. We compare the individual fault orientations from the FPFIT and HASH focal mechanism catalogs with the fault orientations delineated by the relocated earthquakes. We divide these mechanism catalogs into "consistent events" (misfits in strike, dip, and assumed right-lateral slip $\leq 30°$) and "inconsistent events" (misfits of strike, dip, or rake $>30°$). The 30° limit is based on a qualitative comparison of focal mechanisms, fault orientations, and our estimate of how much deviation typical studies using focal mechanism data might be able to tolerate (Fig. 2).

Results

The general trend of the seismicity data, observable even before relocation, indicates that the faults in all three study regions dip steeply and trend northwest–southeast. Using the method outlined in the previous section, we precisely estimate the strike and dip of each fault from relocated data (Table 4; Fig. 3). We do not consider the obvious off-fault earthquakes easily identified in the relocation results (e.g., see Schaff *et al.*, 2002). For the 20-km segment of the Calaveras fault, 3660 earthquakes define a fault with strike N32°W and dip 84°. The 3230 events along a 25-km fault segment of the SAF near San Juan Bautista are consistent with a fault strike of N46W° and dip 85°, and the 665 earthquakes along the Sargent fault show a fault strike of N63°W and a dip of 87°.

For each of the three fault segments, the perpendicular distance from each earthquake to the assumed fault plane does not exceed 800 m. We assume that this implies a single fault plane is a sufficient representation of the data. To confirm this, we also determine the best-fit-fault plane for each relocated multiplet that contains more than 15 earthquakes (26, 35, and 8 multiplets for the Calaveras fault, SAF, and Sargent fault, respectively). These orientations show no systematic offsets and are in agreement with our original estimates based on the full catalogs (i.e., deviations in strike are $\pm 1.6°$, $\pm 1.8°$, and $\pm 5.1°$, and deviations in dip are $\pm 3.9°$, $\pm 7.3°$, and $\pm 8.8°$ for the Calaveras fault, SAF, and Sargent fault data, respectively). These values are well within the range of our assumed 30° uncertainty values (Fig. 2).

Consistent with our fault orientation estimates, the focal mechanism data primarily indicate strike-slip motion on steeply dipping faults (Fig. 4). For both the NCEDC and HASH catalogs, we find no qualitative correlation between the focal mechanism parameters (strike, dip, and rake), location (latitude, longitude, depth), or time. The NCEDC/FPFIT and HASH focal mechanism catalogs, however, are not identical. Comparing events common to both catalogs (785, 1013, and 198 events for the Calaveras fault, SAF, and Sargent fault, respectively), we find that the median angle of rotation between the NCEDC/FPFIT and HASH mechanisms is 33° for the Calaveras fault data, 26° for the Sargent fault data, and 32° for the SAF data. These differences primarily result from differences in fault dip, with the HASH mechanisms having substantially steeper dip than the NCEDC/FPFIT mechanisms (Fig. 4). Previous work shows that the faults in our study region have dips of ~70° or greater e.g., Oppenheimer *et al.*, 1988; Rubin *et al.*, 1999; Schaff *et al.,* 2002), suggesting that the HASH mechanisms are more accurate.

We next examine the agreement between the fault orientations in the NCEDC/FPFIT catalog and the fault orientations delineated by the relocated earthquakes. We find that for all study areas, only 34%–37% of the reported focal mechanisms in the NCEDC/FPFIT catalog are consistent with the fault orientation estimates ($\leq 30°$ difference in strike, dip, and assumed right-lateral rake) based on the relocated data (Table 5). We were initially concerned that these low percentages resulted from the relatively large 250-km source/station distance restriction used in the NCEDC/FPFIT calculations. To test this, we recalculated the mechanisms using a more conservative restriction of 120 km, and found our overall results changed by no more than 10%. This confirms that the poor agreement between the assumed fault orientation and the orientation of the focal mechanism in the FPFIT catalog is not primarily caused by including more distant stations in the calculations. For the focal mechanisms determined by HASH, between 63% and 78% of the mechanisms are consistent (Table 6).

We test how well the various focal mechanism quality parameters generated by NCEDC/FPFIT and HASH (Tables 2 and 3) discriminate between cataloged fault orientations that are consistent or inconsistent with the relocation-based fault orientations. We test various data subsets based on threshold levels of individual quality parameters. For each parameter, we test a range of thresholds and identify the optimal value. We use these distributions to quantify the effectiveness of each parameter. Additional tests could investigate various combinations of the multiple selection criteria, but that is

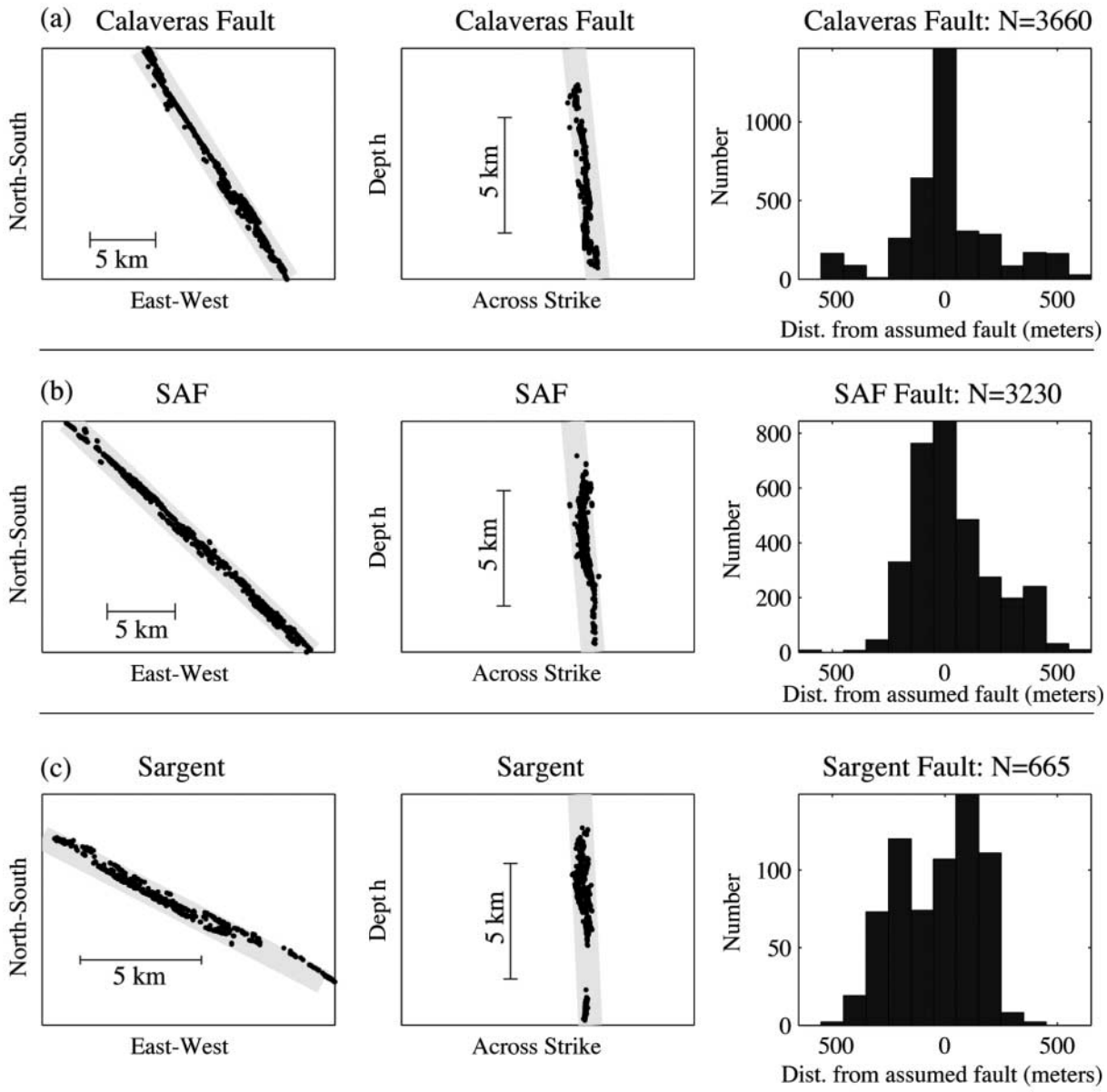

Figure 3. Estimating fault orientations from relocated earthquakes. (a) 3660 relocated earthquakes near the Calaveras fault in map view (left) and cross section (middle). The thickness in map view is from a slight fault dip. The deviation from the best-fit fault plane, as determined by principal component analysis, is also shown (right). (b) As in (a) but for data from 3230 earthquakes along the San Andreas fault. (c) As in (a) and (b) but for data from 665 earthquakes along the Sargent fault. For all three datasets, the deviation from the best-fit fault does not exceed 800 m.

beyond the scope of this paper and is likely to be very dataset and project goal dependent.

We evaluate how useful each catalog parameter is for identifying quality mechanisms, using trade-off curves to evaluate the number of mechanisms that exceed various threshold values, as a percent of the mechanisms deemed consistent with the fault orientation from the relocated earthquakes (Fig. 5). If a parameter is useful, a negative relationship exists between the number of mechanisms and the percent consistent, such that increasing the strictness of the threshold improves the dataset quality. Uniformity of these tests allows us to evaluate if one parameter is more useful than another by comparing the height of each trade-off curve. The higher the trade-off curve, the more productive the parameter is for identifying quality mechanisms, meaning that for similar-sized datasets, a larger fraction of the data is high quality, or that a larger dataset can be produced with similar quality. For instance, in Figure 5a, the trade-off curve for the STDR parameter is higher than the trade-off curve for the magnitude parameter, indicating that STDR

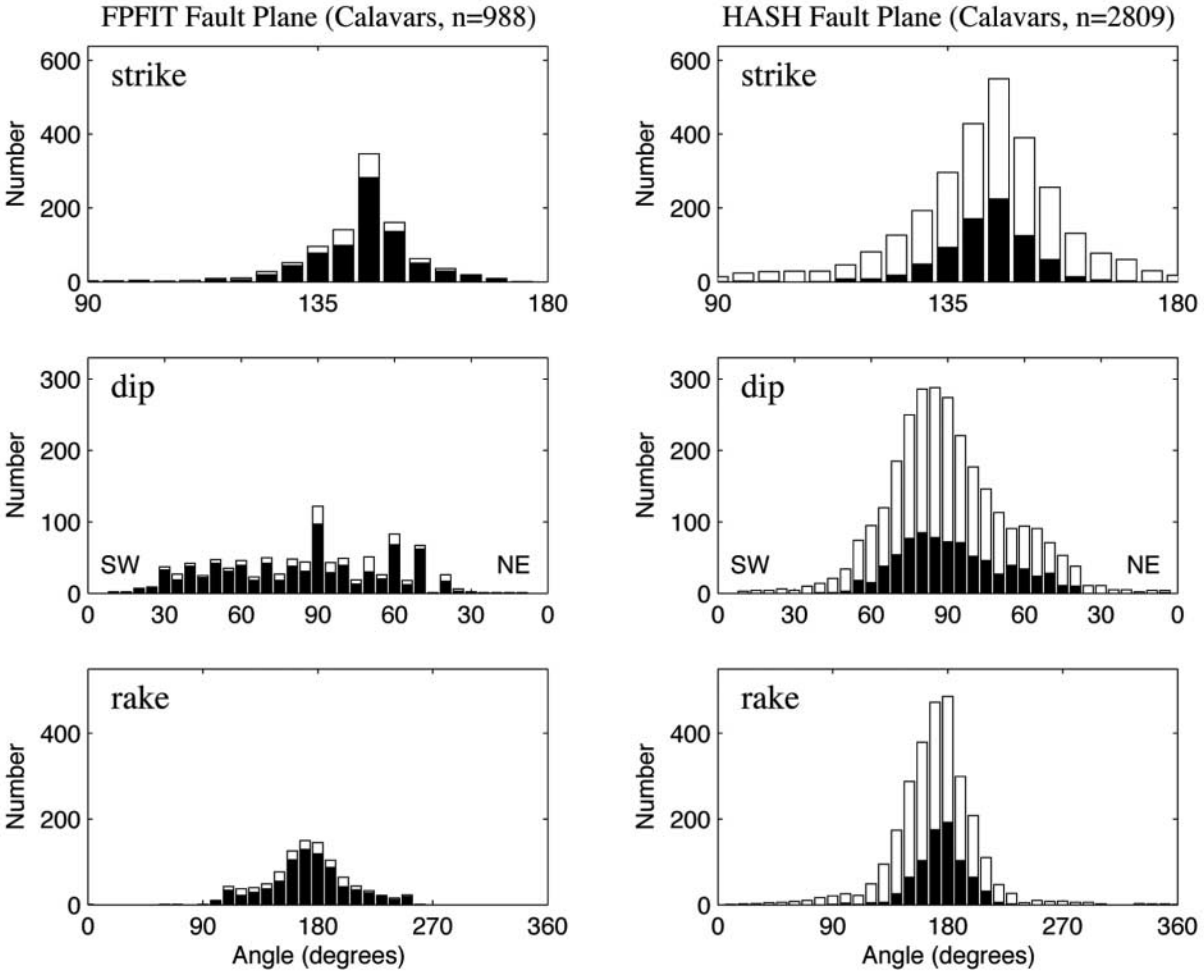

Figure 4. Histograms of focal mechanism parameters (strike, dip, and rake) in the NCEDC/FPFIT (left column) and HASH (right column) catalogs for the relocated Calaveras data. We only consider mechanisms in the FPFIT catalog that do not have multiple solutions, thus the numbers of events in each catalog differ (988 in the FPFIT catalog; 2809 in the HASH catalog). Of these, 785 are common to both catalogs (indicated by the solid filled histograms) and exhibit the same overall pattern as the full catalogs. The peaks in the histograms indicate strike-slip motion on steeply dipping faults for all regions.

does a better job of separating quality FPFIT mechanisms without substantially reducing the final catalog size. A parameter is not useful for identifying quality mechanisms if the curve is flat (or has a positive slope), indicating no relation (or a positive relation) between the number of mechanisms and the percent of the mechanisms consistent with the assumed fault orientations.

We choose an optimal threshold value for each parameter by inspecting the trade-off between dataset size and the percent of consistent mechanisms (Fig. 5). We assume the parameter constraint is too stringent if the chosen dataset is reduced to 20% or less of the original size. We also consider the parameter constraint too ineffective if the chosen dataset does not contain at least 50% of the "correct data." The latter case assumes that the dataset contains less than 50% quality mechanisms initially; if the entire dataset is higher quality than that, we will consider any parameter constraint that decreases the percent misfit by at least a third to be an adequately useful constraint.

We find that for the NCEDC/FPFIT catalogs, the most reliable mechanisms have a high percentage of nonnodal stations, quantified by the STDR parameter (Table 5, Fig. 5a). The STDR parameter is a measure of how the stations are distributed about the focal sphere, where values of 1 and 0 indicate good and bad distributions, respectively. STDR is sensitive to how the stations are distributed throughout the region and to the focal mechanism (i.e., the STDR might change if the earthquake and station locations remain fixed but the focal mechanism changes orientation). In particular, a low STDR indicates that many of the polarity observations come from near-nodal stations, where direct *P* arrivals are of small amplitude, making it difficult to identify and assess

Table 5
Fault Orientations and Assumed Slip Direction Determined from the Relocated Microearthquakes Compared with Corresponding Focal Mechanisms from NCEDC/FPFIT Catalog

Fault Segment	Number of Focal Mechanisms	Number of "Consistent" Mechanisms (FPFIT catalog)	% "Consistent" (FPFIT catalog)	Constraint
Calaveras	988	364	37%	None
	887	363	41%	STDR $>$ 0.50
	350	237	68%	STDR $>$ 0.65
	237	122	51%	Mag $>$ 2.0
	185	56	30%	ΔSTR $<$ 30°
				ΔDIP $<$ 30°
				ΔRAK $<$ 30°
San Andreas	1025	349	34%	None
	921	349	38%	STDR $>$ 0.50
	296	190	64%	STDR $>$ 0.65
	388	150	39%	Mag $>$ 2.0
	197	44	22%	ΔSTR $<$ 30°
				ΔDIP $<$ 30°
				ΔRAK $<$ 30°
Sargent	208	71	34%	None
	201	71	35%	STDR $>$ 0.5
	83	52	63%	STDR $>$ 0.65
	30	15	50%	Mag $>$ 2.0
	33	5	15%	ΔSTR $<$ 30°
				ΔDIP $<$ 30°
				ΔRAK $<$ 30°

The comparison is considered a match ("consistent") if the deviation in the expected strike/dip/rake is less than or equal to 30°. For the original catalogs, no more than 37% of the focal mechanisms are consistent with the expected fault orientations. Restricting the data to STDR $>$ 0.65 increases these percentages to 63%–68%.

the first-motion polarity. The STDR is derived from information from each station, yet the number of stations does not play as primary a role in the STDR parameter as how the stations are spatially distributed. We find that requiring STDR $>$ 0.65 (acceptable range 0.58–0.7) is the most effective way to identify quality mechanisms in the NCEDC/FPFIT catalogs. If the criteria of STDR $>$ 0.65 is used, ~63%–68% of the chosen mechanisms are in agreement (errors in strike, dip, and rake $\leq$30°) with the fault orientations revealed by the relocated seismicity (68% for the Calaveras fault, 64% for the SAF, and 63% for the Sargent fault).

For the HASH catalog, the FPU is the most robust estimate of quality focal mechanisms. FPU is derived from the variability in the set of acceptable solutions for each event, determined using a Monte Carlo technique that accounts for variations in velocity model and earthquake depth (Hardebeck and Shearer, 2002). Specifically, if the rms angular difference between the acceptable solutions and the preferred solution is less than or equal to 35° (acceptable range ~30°–45°), higher-quality mechanisms are obtained (Fig. 5c; Table 6). With the criterion of FPU $\leq$ 35°, more than 80% of the mechanisms agree with the fault orientations determined from the relocated seismicity (82% for the Calaveras fault, 81% for the SAF, and 83% for the Sargent fault). Interestingly, the STDR does not appear to be as useful a discriminant for the HASH results as it was for the NCEDC/FPFIT catalog. Requiring STDR $>$ 0.65 tends to eliminate most of the mechanisms without improving the percent accuracy for the HASH catalog.

Overall for the NCEDC/FPFIT catalog, the parameter constraints that increase the percentage of consistent mechanisms, while simultaneously not reducing the overall number of mechanisms, include the following: STDR (>0.65 preferred; range 0.58–0.70), number of weights greater than 0.1 (>65 preferred; range 60–70), the event magnitude (>2.1 preferred; range 1.9–2.2), and the number of observations (>60 preferred; range 55–70) (Fig. 5a). The best discriminators for the HASH catalog (Fig. 5c) include FPU ($\leq$ 35° preferred; range 30°–45°), azimuthal gap (<70° preferred; range 50°–90°), number of observations (>20 preferred; range 12–25), and magnitude (>1.5 preferred; range 1.1–1.7).

We similarly test how well the assumed cataloged uncertainties in strike, dip, and rake reflect what we expect are the true uncertainties. We find that restricting the NCEDC/FPFIT focal mechanism data to only mechanisms that have uncertainties in strike, dip and rake less than or equal 30° does not improve the catalog, as the percentage of correct mechanisms falls from the already low values of 34%–37% to 15%–30% (Table 5 and Fig. 5b). This suggests that the uncertainty estimates reported to be less than 30° in the NCEDC/FPFIT catalog are in fact much higher than 30°.

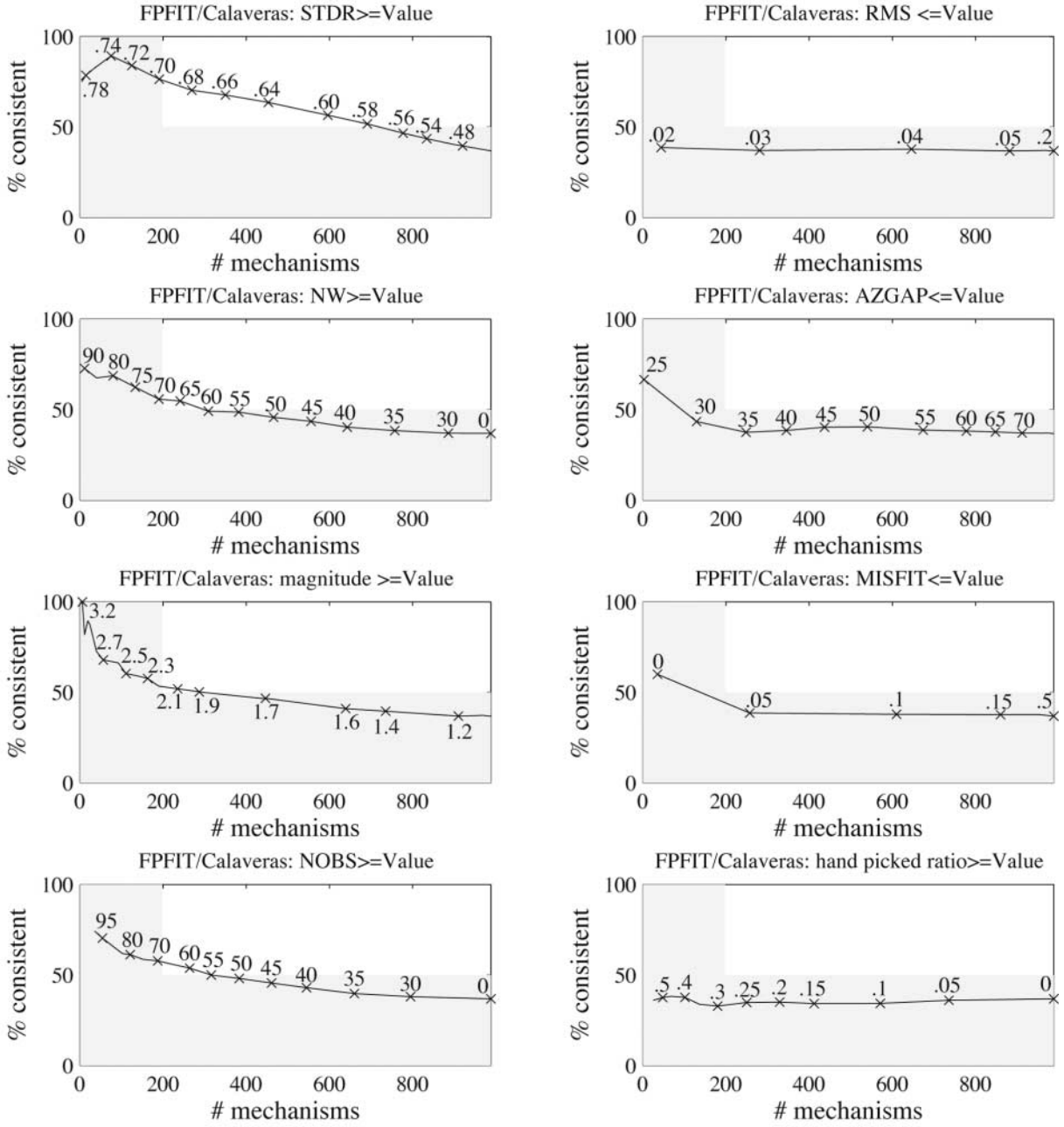

Figure 5. (a) Evaluation of quality parameters in the NCEDC/FPFIT catalog (see Table 2 for definitions). We determine a trade-off curve that tracks the percentage of consistent focal mechanisms in the data subset (*y* axis) as a function of the number of events in the subset (*x* axis). Threshold values for each parameter (small numbers along the curves) limit which focal mechanisms are included in the subset. Shaded areas indicate the data subset is either too small or too inaccurate to be acceptable (<20% of the data set remains or >50% of the data is expected to be incorrect). A trade-off curve with a negative slope indicates that the parameter restrictions improve the data quality. A higher curve indicates a more successful parameter. Parameters that most easily separate consistent mechanisms from inconsistent mechanisms (high percentage of consistent mechanisms obtained), while simultaneously not eliminating too much of the data, are the STDR, number of weights (NW), magnitude, and number of observations (NOBS) (left column). Parameters that are not as successful at reducing the data to consistent mechanisms include rms, AZGAP, MISFIT, and the ratio of hand-picked/machine-picked first motions (right column). (*continued*)

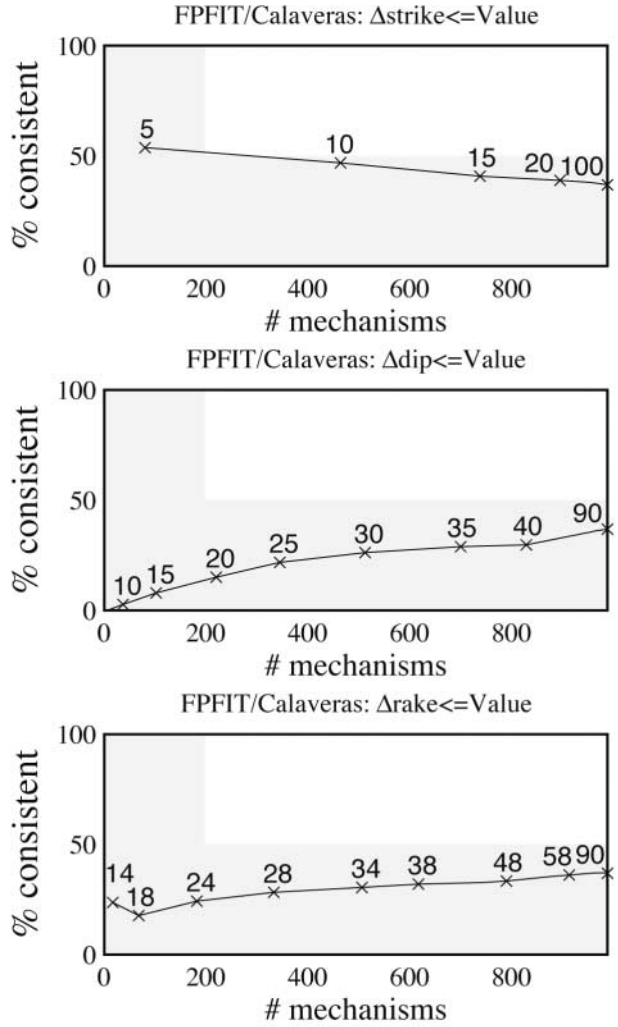

Figure 5. (continued) (b) As in (a) to test the formal misfit reported in the NCEDC/FPFIT catalog of the strike, dip, and rake. For the NCEDC/FPFIT catalog, formal mechanism uncertainty does a poor job of separating consistent from inconsistent mechanisms. (*continued*)

HASH does better, with median angular difference of the acceptable fault planes from the preferred plane (FPU) listed in the HASH catalog of 32°–40°, compared to the median true misfit that is 20°–25°. This indicates that the uncertainties reported in the HASH catalog are relatively conservative.

Next, we quantitatively investigate the relationship between the cataloged uncertainty estimates (i.e., errors in strike, dip, and rake) and the actual misfit values based on our assumed fault orientation (Fig. 6). We assign a normalized misfit, equal to the actual misfit divided by the catalog uncertainty estimate, to each cataloged focal mechanism. For a perfect catalog, the plot of the confidence level C ($0 \leq C \leq 1$) versus the fraction of events with misfit less than C, is a straight line with a slope of 1 (i.e., 68% of mechanisms are correct to within their 1-sigma uncertainty, 95% to within their 2-sigma uncertainty, etc.). If the cataloged uncertainty estimates are too small, the curve will fall below this line, and if the uncertainty estimates are too large, the curve will be above this line.

We first evaluate the confidence values for only the data assumed to be high quality (i.e., errors $\leq$30°), which eliminates at least 65% of the data in the FPFIT and HASH catalogs. Evaluating the normalized misfit for each mechanism parameter (strike, dip, rake) separately, the HASH uncertainty estimates are slightly more robust than the FPFIT estimates (Fig. 6a, dashed lines). If instead, we assume a mechanism is correct to within the confidence region only if all the focal mechanism parameters (strike, dip, rake) are correct to within their respective uncertainties (i.e., a single parameter test), we find the HASH results remain approximately the same, but the FPFIT results are substantially worse (Fig. 6a, solid lines). We repeat these tests using the full data catalogs (Fig. 6b). Generally, this tends to slightly degrade the HASH results and improve the FPFIT results. However, most of this FPFIT success results from cataloged mechanisms that are reported to, and do indeed, have very large uncertainties, which is not as favorable as a catalog with correctly estimated small uncertainties. We conclude that the HASH uncertainty estimates reflect the uncertainty of the entire mechanism (strike, dip, rake), while the FPFIT uncertainty estimates reflect single-parameter uncertainty. Since we assume that a mechanism is correct only if the strike, dip, and rake are all correct to within 30°, the HASH uncertainty estimates are more appropriate for our purposes.

We next test the common assumption that larger-magnitude (e.g., $M > 2$) earthquakes have more accurate focal mechanisms. This is based on the idea that larger-magnitude earthquakes have stronger seismic signatures that are well above the noise, which can be recorded at more, and further away, stations. Our aim is to determine if the 655 and 828 earthquakes in the NCEDC/FPFIT and HASH catalogs, respectively, that exceed magnitude 2, have the highest-quality focal mechanisms. We find 39%–51% of the NCEDC/FPFIT catalog and 83%–88% of the HASH catalog are consistent with the expected orientations revealed in the relocated data. These percentages are an improvement over those in the original catalog, indicating that the $M > 2$ earthquakes have more accurate focal mechanisms than the smaller events. However, restricting the data to these larger events drastically reduces the number of focal mechanisms available (only 10%–15% of the original data contains large-magnitude events), making this method of data refinement not as favorable as other methods (Tables 5 and 6). Studies that incorporate a large number of small-magnitude mechanisms are not necessarily flawed by systematic bias in orientation but may overestimate the variability of fault orientations and could suffer from large uncertainties.

For our final test, we use a cluster of 11 "repeating earthquakes" on the Calaveras fault (located at approximately $-121.64°$, 37.26°, 6-km depth) to gauge the accuracy of the cataloged earthquake focal mechanisms. Repeating earthquakes, by definition, rupture identically oriented fault

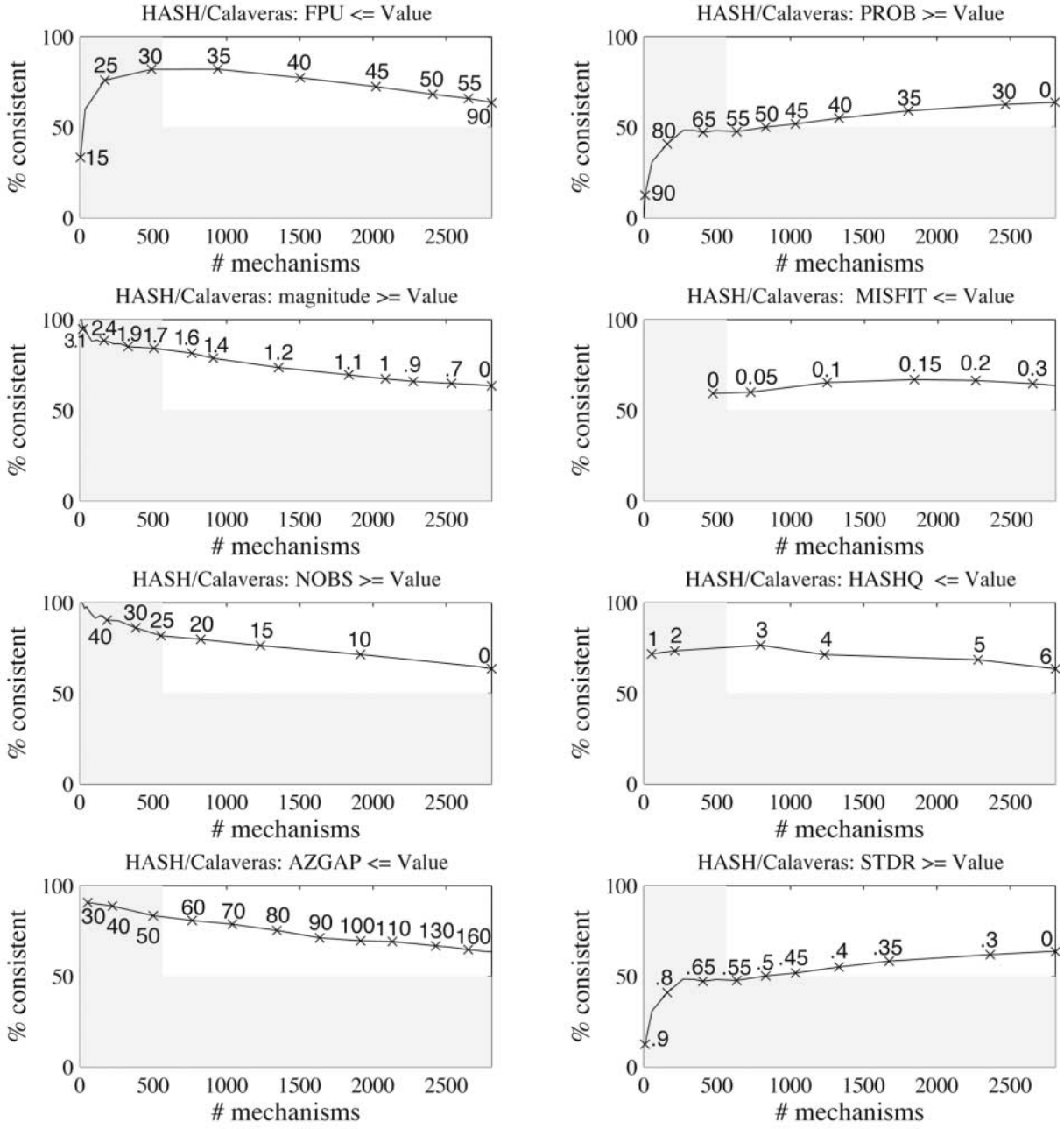

Figure 5. (continued) (c) As in (a) but for data in the HASH catalog (see Table 3 for parameter definitions). For these data the parameters that best separate consistent mechanisms from inconsistent mechanisms are FPU, magnitude, NOBS, and AZGAP (left column). Restrictions on parameters MISFIT, HASH-Q, and STDR are not as successful (right column).

planes (Nadeau and McEvilly, 1999; Rubin, 2002a; Schaff *et al.*, 2002), and so our expectation is that each of the focal mechanisms for these 11 quakes should be identical or very similar. We find the HASH mechanisms exhibit much more similarity with each other than the NCEDC/FPFIT mechanisms (Fig. 7; Table 7). Since the waveforms of these earthquakes are virtually identical at each station, implying identical focal mechanisms, this suggests the HASH catalog is more reliable. Similar tests using other groups of repeating earthquakes also favor the HASH mechanism catalog over the FPFIT mechanism catalog (Ⓔ See supplemental material available in the electronic edition of BSSA.)

Discussion

How Good Are First Motion Focal Mechanism Data?

The NCEDC/FPFIT focal mechanism datasets examined in this study can, on average, predict the correct overall trend and dip of the main fault orientation for each study region

Table 6
As in Table 5 but for Results from the HASH Focal Mechanism Catalog

Fault Segment	Number of Focal Mechanisms	Number of "Consistent" Mechanisms (HASH catalog)	% "Consistent" (HASH catalog)	Constraint
Calaveras	2809	1783	63%	None
	464	222	48%	STDR $>$ 0.60
	941	772	82%	FPU $\leq$ 35°
	276	239	87%	Mag $>$ 2
San andreas	2396	1815	76%	None
	188	157	84%	STDR $>$ 0.60
	1548	1257	81%	FPU $\leq$ 35°
	520	433	83%	Mag $>$ 2
Sargent	400	314	78%	None
	96	71	74%	STDR $>$ 0.60
	257	214	83%	FPU $\leq$ 35°
	32	28	88%	Mag $>$ 2

For the original catalogs, 63%–78% of the mechanisms are consistent with the expected fault orientation; constraining the data to FPU $\leq$ 35° increases the percentage to 81%–83%.

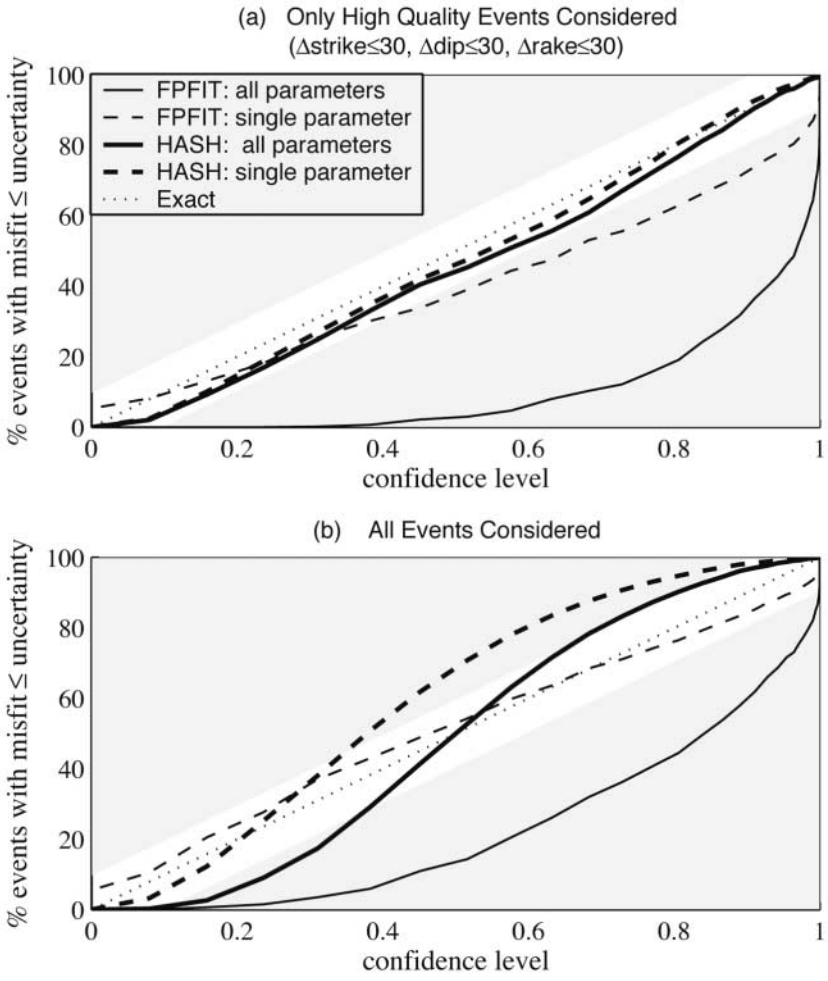

Figure 6. Assessing the quality of the cataloged formal uncertainty parameters (errors in strike, dip, and rake) based on the observed misfit to the fault orientations delineated by the relocated earthquakes. (a) Evaluation of the FPFIT (thin lines) and HASH (thick lines) catalog estimates of the uncertainties in strike, dip, and rake for high-quality data (i.e., errors in strike, dip, and rake $\leq$30°). For reference, a perfect estimate of the uncertainties is shown with the linear dotted line and preferred values fall in the nonshaded regions. If the uncertainty estimates are too small, the curve is below this line, and if the uncertainty estimates are too large, the curve is above this line. Dashed lines: each mechanism parameter (strike, dip, rake) is considered separately. Solid lines: a mechanism is considered correct to within the confidence region only if all three of the parameters are correct to within their respective uncertainties. (b) As in (a) but includes all data listed in the catalogs.

(e.g., Oppenheimer *et al.*, 1988). Yet, any attempt to more specifically assign strike/dip parameters to within less than 30° for individual earthquakes would be in error for >70% of the data if only the cataloged errors in the strike, dip, and rake parameters (ΔSTR, ΔDIP, and ΔRAK, Table 5) were used to identify the expected high-quality mechanisms. What is more, these constraints eliminate a substantial portion of the data without a significant increase in the data quality (Fig. 5a).

The uncertainty estimates in the catalog generated by HASH appear to be better suited for identifying quality mechanisms than those generated by NCEDC/FPFIT because they are a more useful indicator of mechanism accuracy (Figs. 5 and 6). Our results indicate that HASH's mechanism stability parameter (i.e., FPU) is a reasonably robust test of mechanism quality. Future tests are needed to validate these findings for fault systems that include normal and reverse faulting environments or strike-slip faulting in regions where the velocity structure is relatively unknown. In the thrust-faulting 1994 Northridge, California, earthquake sequence, Shearer *et al.* (2003) found many HASH focal mechanisms to be in agreement with the planes defined by relocated similar event clusters, indicating that the type of analysis presented here can be extended to other tectonic regimes.

Our tests indicate that focal mechanism catalogs created using FPFIT are useful, when appropriate quality control is enforced to help identify and extract individual high-quality mechanisms. In particular, for the NCEDC/FPFIT catalog, STDR > 0.65 is the most reliable discriminator of accurate focal mechanisms while still maintaining a sufficient quantity of data. Ideally we should put more stations off known fault traces and strive for more uniform station spacing, so that good station coverage exists throughout the focal sphere. If the source/station distance becomes too large, additional complications arise if the *Pn* phase arrives before the *P* phase. Knowing which phase arrives first is important because in some situations the *Pn* and *P* phases have opposite polarities and/or different takeoff angels. The fact that our overall FPFIT results are not significantly changed (deviations <10%) when the restriction on the source/station maximum distance of 250 km (the value used to create the existing online catalog) is reduced to 120 km indicates that errors introduced from the more distant stations are not significant.

In some studies, accounting for errors in the strike, dip, and rake measurements is crucial (e.g., Aagaard *et al.*, 2004). One way to estimate uncertainties in these parameters it to compare the results from different accepted focal mechanism catalogs and assume that the deviations between the cataloged parameters represent the true uncertainties. Applying this method to the NCEDC/FPFIT and HASH catalogs, a median 3D angular rotation of 26°–33° is needed to align the mechanisms. These values are within the limits of the 18°–38° 3D rotation angles Kagan (2000) found in event

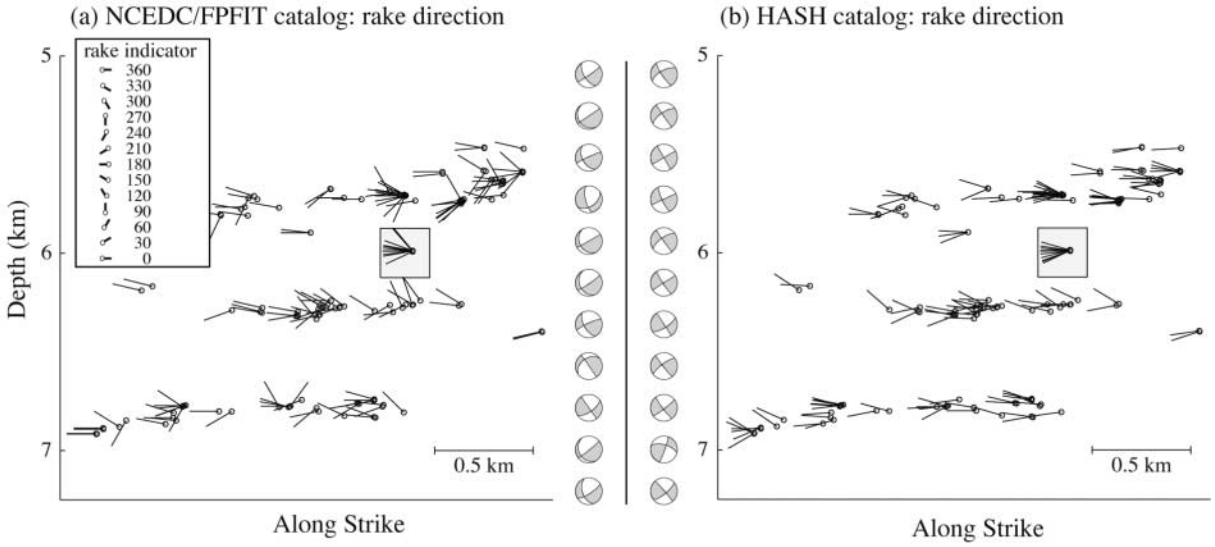

Figure 7. Study of 11 "repeating earthquakes" on the Calaveras fault (approximate location: 37.26°, −121.64°, depth 6 km) that are expected to have identical focal mechanisms (e.g., see Schaff *et al.*, 2002). (a) Cross section of a portion of the Calaveras fault with indicators of the NCEDC/FPFIT focal mechanism rakes for this region (short lines). The 11 repeating earthquakes (within the shaded box) have focal mechanisms with a substantial degree of variation (mechanisms shown, see Table 7 for more details). (b) As in (a) but for data reported in the HASH catalog. The 11 HASH mechanisms show the more expected minimal mechanisms' variability. (The NCEDC event ID numbers of the 11 earthquakes in the repeating sequence, from top to bottom, are 16518, 19603, 22813, 27874, 36639, 51809, 77721, 112665, 139159, 314251, and 30072461).

Table 7
Focal Mechanisms for Events in the Repeating Cluster of Earthquakes Shown in Figure 7

Strike (328° expected)	Dip (84° expected)	Rake (±180° expected)	Method	Event ID
326°	102°	155°	HASH	16518
325°	92°	158°	HASH	19603
330°	90°	189°	HASH	22813
335°	102°	179°	HASH	27874
324°	92°	158°	HASH	36639
327°	97°	179°	HASH	51809
327°	89°	160°	HASH	77721
322°	95°	165°	HASH	112665
323°	98°	−174°	HASH	139159
286°	61°	174°	HASH	314251
319°	87°	164°	HASH	30072461
328°	120°	−174°	NCEDC/FPFIT	16518
325°	160°	180°	NCEDC/FPFIT	19603
331°	130°	173°	NCEDC/FPFIT	22813
347°	111°	−131°	NCEDC/FPFIT	27874
330°	150°	180°	NCEDC/FPFIT	36639
334°	150°	−170°	NCEDC/FPFIT	51809
330°	120°	170°	NCEDC/FPFIT	77721
325°	90°	−130°	NCEDC/FPFIT	112665
325°	90°	155°	NCEDC/FPFIT	139159
330°	155°	−170°	NCEDC/FPFIT	314251
340°	130°	−160°	NCEDC/FPFIT	30072461

Because the waveforms of these earthquakes are almost identical, we expect the mechanisms to also be similar. The HASH mechanisms exhibit more similarity with each other than the FPFIT mechanisms, especially in dip, indicating the HASH catalog is more robust. (Ⓔ Additional quality parameters for these events is available in the electronic edition of BSSA.)

pairs in the Harvard CMT catalogue that had small time/space intervals. This implies that modern day focal mechanism catalogs have median uncertainties in strike, dip, and rake that typically do not exceed 40°. Without studies such as this one, it is difficult to determine if variations in catalogs such as these are attributed to true differences in the fault orientations (as in Fig. 2) or if they solely represent measurement errors.

Erroneous first-motion polarity data can result from refractions of seismic waves from unmodeled 3D velocity structures and/or strong velocity changes across the fault zone (e.g., Oppenheimer *et al.*, 1988; Ben-Zion and Malin, 1991; Igel *et al.*, 2002). As both the SAF and the Calaveras fault have relatively high (~20%) cross-fault velocity contrasts (e.g., Eberhart-Phillips and Michael, 1998; Dorbath *et al.*, 1996; Rubin *et al.*, 1999), it is possible that a contributing cause of the spurious mechanisms in both the NCEDC/FPFIT and HASH catalogs is unmodeled velocity structure. The HASH datasets were tested for focal mechanism sensitivity to velocity model, but only for differences between 1D velocity structures. Many indications show that 1D velocity models are inappropriate for these regions, including the multiple NCSN 1D velocity models in this region (e.g., LOM, LON, COY, TRE) that, in combination, create a complex 3D structure (Oppenheimer *et al.*, 1993). Pertinent to our study region, Oppenheimer *et al.*, (1988) suggest that the resulting 80°–85° dip of the Calaveras fault (which is consistent with the 84° dip in this study) in their study might be caused by an unmodeled lateral refraction across the Calaveras fault, and instead, the true dip is 90°. Sensitivity of the cataloged focal mechanisms in the NCEDC/FPFIT and the HASH catalogs to complex 3D structure should be tested in the future. However, the many fault-aligned mechanisms in the NCEDC/FPFIT and HASH datasets indicate that quality focal mechanisms can be derived even in the presence of unmodeled 3D velocity structure.

The FPFIT computer program has an associated 1985 manual (Reasenberg and Oppenheimer, 1985), which contains cautionary warnings and the potential pitfalls of blindly using the FPFIT results. The authors of the original code foresaw and documented potential problems illustrated by the warning in the FPFIT manual in the section on "Estimation of Parameter Uncertainty and Solution Quality" that discusses the STDR: "STDR is the station distribution ratio ($0.0 \leq \text{STDR} \leq 1.0$). This quantity is sensitive to the distribution of the data on the focal sphere, relative to the radiation pattern. When this ratio has a low value (say, $\text{STDR} < 0.5$), then a relatively large number of the data lie near nodal planes in the solution. Such a solution is less robust than one for which $\text{STDR} > 0.5$, and, consequently, should be scrutinized closely and possibly rejected" (Reasenberg and Oppenheimer, 1985). Over the years since its inception, experience with focal mechanism catalogs generated by FPFIT allowed Hardebeck and Shearer (2002) to design a technique

to improve focal mechanisms and more accurately characterize their uncertainty. As seismic recording improves, and experience with the HASH computer code develops, more improvement in focal mechanism quality will occur.

Effect of Erroneous Focal Mechanism Data on Seismic Hazard Estimates

Pinpointing future large and damaging earthquake locations is a continual goal of the seismological community. Identifying which measurable parameters, if any, can help identify impending large earthquakes or large aftershocks is the focus of multiple studies (e.g., Das and Scholz, 1981; Harris, 1998 and references therein; Felzer *et al.*, 2003; Tibi *et al.*, 2003; Toda and Stein, 2003). With technology advancements (e.g., larger computer memory, faster data transfer speeds, and increases in computational efficiency), theoretical seismic hazard analyses can incorporate more intricacies in the models. The question becomes, what should we be modeling in more detail? For example, do we need exact fault orientations of small-magnitude earthquakes, or to derive a more accurate 3D seismic velocity structure?

One branch of study assumes that knowledge of the fault orientations is inconsequential to seismic hazard analysis, and instead the best indicators of heightened odds of large earthquakes come from the locations and magnitudes of earthquakes (e.g., Wyss and Wiemer, 2000; Gerstenberger *et al.*, 2001; Wiemer and Wyss, 2002; Imoto, 2003). Given this, refined estimates of a regional 3D velocity model or detailed fault orientations do not improve hazard analyses. The improvement comes instead by adding additional seismic networks to reduce the magnitude of completeness in the catalogs.

A second branch of study uses theoretical stress changes from large mainshocks to predict regions of heightened odds of large magnitude aftershocks or future mainshocks (e.g., King *et al.*, 1994; Toda *et al.*, 1998; Stein, 1999; Brodsky *et al.*, 2000; Anderson *et al.*, 2003; King and Bowman, 2003). These computations are complicated by the fact that these stress change maps, and in turn hazard estimates, are highly dependent on the fault orientation and slip directions of the causative mainshock and the recipient aftershocks (e.g., Belardinelli *et al.*, 1999; King and Cocco, 2001; Harris and Simpson, 2002; Kilb, 2003). Additional complexity can be caused by kinks and undulations in the earthquake fault planes. Although the existence of this complexity is well known, it is currently difficult to accurately map in fine-scale detail because the uncertainties can be large. Simplified assumptions, such as optimally oriented faults, help avoid these complications. Unfortunately, these simplifications may not sufficiently represent the true fault orientations (Kilb *et al.*, 1997; Hardebeck *et al.*, 1998) or significantly alter the overall results.

If seismic hazards can be estimated from stress change calculation, the techniques in this study could reduce errors in fault orientation parameters that would help reduce the overall uncertainties in the hazard estimations. Given certain fault geometries, relatively small errors (~30°) in fault parameters can yield very large uncertainties in static stress change calculations, which can produce contradictory results (Fig. 8). A study by Harris and Simpson (2002) of the influence of stress changes from the 1992 M 7.2 Landers, California, earthquake at the site of the 1999 M 7.1 Hector Mine, California, earthquake finds results varying from a ~0.3 MPa stress increase (triggering expected) to a ~0.3 MPa stress decrease (triggering not expected) at that location when using different proposed fault models. King and Cocco (2001) find that, generally, stress changes derived on steeply dipping strike-slip faults are most sensitive to the strike of the fault planes and least sensitive to variation in the dip of the fault plane. Similarly, Kilb *et al.* (2002) found that for vertical strike-slip mainshocks, the mapped pattern of the static and dynamic stress change is sensitive to aftershock fault strike variations for which the stresses are derived. As the strike of the aftershock fault plane rotates clockwise, the mapped stress pattern is rotated clockwise about the mainshock fault (see Fig. 9 of Kilb *et al.*, 2002). Results based on inaccurate fault parameters can correspondingly be in error, potentially leading to incorrect hazard estimations.

Conclusions

We constrain the strike and dip of three California fault segments (Calaveras, Sargent, and a portion of the San Andreas near San Juan Bautista) using principle component analysis of accurately located microearthquakes, as determined from cross correlation of their seismic waveforms. We assume these orientations reflect the true fault geometries and use these results to test the quality of two different focal mechanism catalogs: NCEDC/FPFIT (Reasenberg and Oppenheimer, 1985) and HASH (Hardebeck and Shearer, 2002). The primary difference between these catalogs is that the code used to create the HASH catalog estimates the mechanism quality from the solution stability with respect to the uncertainty in the input parameters (velocity model, earthquake location, and polarity measurements), whereas FPFIT does not.

For each focal mechanism, in each catalog, we assign a grade of "consistent" if the mechanism deviates by no more than 30° from the true strike, dip, and assumed right-lateral slip, and "inconsistent" otherwise. Using this assignment, we can judge the quality of the catalogs. We find the focal mechanisms in the original NCEDC/FPFIT catalog have a "consistent" grade of 37%, 34%, and 34% for the Calaveras fault, SAF, and Sargent fault, respectively, whereas the corresponding values for the HASH catalog are 63%, 76%, and 78%. Therefore, we expect the diversity in the focal mechanism data predicted by the NCEDC/FPFIT catalog to be in error, and we suggest that the HASH technique improves the computed focal mechanisms.

For the NCEDC/FPFIT catalog, the more reliable mechanisms are those determined from primarily nonnodal sta-

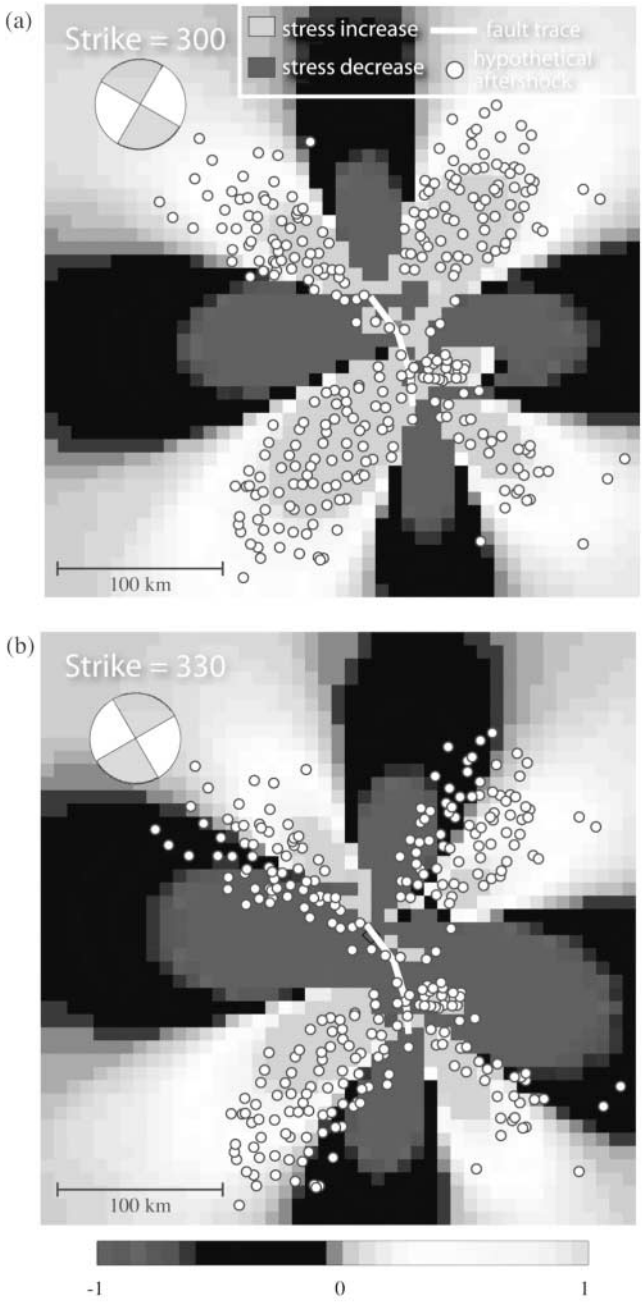

Figure 8. Sensitivity of static Coulomb stress change to the assumed aftershock fault orientations on which the stresses are derived. (a) Static Coulomb stress changes (gray-scale shading) from a mainshock fault system (three white line segments representing the 1992 M 7.2 Landers earthquake) derived on vertical aftershock faults that strike 300° and have a right-lateral component of slip. (b) As in (a) but the aftershock fault orientations strike at 330° instead of 300°. Hypothetical aftershock locations (white circles) locate in the same locations in (a) and (b) with the purpose to highlight the sensitivity of Coulomb stress change to the assumed aftershock fault orientations. Note that this small 30° change in aftershock strike drastically reduces the correlation between regions of Coulomb stress increase (lighter regions) and the hypothetical aftershock locations. This figure is a simple illustration of how much error can be introduced in static Coulomb stress change studies (i.e., we do not suggest that real datasets contain uniform errors).

tions, so in the absence of clear fault orientations (surface rupture, obvious delineation by microearthquakes), focal mechanisms that have a STDR greater than 0.65 are the most reliable. Although this does not ensure that the data will be error free, using this criterion eliminates the largest percentage of incorrect mechanisms while maintaining a large portion of the data. The original 1985 FPFIT documentation states that the STDR is a useful parameter, but the STDR being the most useful parameter is unexpected.

For the HASH mechanisms, the most useful criterion for discriminating between good and bad mechanisms is the 1-sigma FPU. A threshold of FPU $\leq 35°$ leads to ~80% correct mechanisms. For both catalogs (NCEDC/FPFIT and HASH), restricting the first-motion focal mechanism data to only larger-magnitude events (e.g., $M > 2$) ensures higher-quality focal mechanisms (39%–51% for NCEDC/FPFIT and 83%–88% for HASH), at the expense of eliminating a large portion of the data (Table 5).

For the FPFIT and HASH catalogs, it is possible that some of the errors in the focal mechanism parameters result from unmodeled variable 3D-velocity structure in the region, but further work is needed to fully test this hypothesis. For the FPFIT catalog, many of the erroneous focal mechanism data result from a poor distribution of stations that do not adequately cover the focal sphere. We find that the FPFIT solutions are not significantly changed when the current maximum 250-km source/station distance restriction (used to compute solutions in the current catalog) is reduced to 120 km. The high rate of focal mechanism error indicates that the "user-beware" warnings and the cautionary remarks in the 1985 FPFIT manual (Reasenberg and Oppenheimer, 1985) should be followed.

In summary, the results of this study show that (1) focal mechanism catalogs generated using HASH are more accurate than those generated from FPFIT; (2) the high-quality mechanisms from FPFIT catalogs can be identified by requiring the STDR to be above 0.65; (3) the high-quality mechanisms from the HASH catalog can be identified by requiring the FPU to be less than or equal to 35%; (4) determining fault orientations using relocated data is the preferred way to estimate large-scale fault orientations; and (5) formal mechanism uncertainty as a good discriminator of accurate mechanisms validates the HASH approach of using mechanism stability as a measure of solution quality.

Acknowledgments

We thank Allan Rubin for supplying us with his relocated datasets and J. L. Got for his relocation code. This work would not have been possible with out data from the Northern California Earthquake Data Center (NCEDC) and the work contributed by Northern California Seismic Network, U.S. Geological Survey, Menlo Park, and the Berkeley Seismological Laboratory, University of California, Berkeley. This study benefited from helpful discussions with Yehuda Ben-Zion, the Princeton Seismology group, Peter Shearer, and Frank Vernon. David Oppenheimer, Stephanie Prejean, Felix Waldhauser, Stephan Wiemer, and an anonymous reviewer provided helpful comments on the manuscript. We also thank Jennifer Ma-

thews for helping us refine some of our figures and Judy Gaukel for helping us edit the final manuscript. Essential to the creation of the 3D visualizations was work by Atul Nayak and Charles Zhang and support from Jason Leigh and the SIO Visualization Center. D.K. was supported by the NSF OptIPuter project (ITR Cooperative Agreement SCI-0225642), and J.L.H. was supported by the USGS Mendenhall postdoctoral program.

References

Aagaard, B. T., J. F. Hall, and T. H. Heaton (2004). Effects of fault dip and slip rake angles on near-source ground motions: why rupture directivity was minimal in the 1999 Chi-Chi, Taiwan, earthquake, *Bull. Seism. Soc. Am.* **94,** 155–170.

Abercrombie, R. E., T. H. Webb, S. Bannister, R. Robinson, J. Beavan, and T. Arnadottir (1996). The enigma of the Arthur's Pass earthquake (abstract), *EOS Trans. AGU*, **77,** no. 22 (West. Pac. Geophys. Meet. suppl.), W90.

Abercrombie, R. E., T. H. Webb, R. Robinson, and P. J. McGinty (2000). The enigma of the Arthur's Pass, New Zealand, earthquake, 1: Reconciling a variety of data for an unusual earthquake sequence, *J. Geophys. Res.* **105,** 16, 119–16, 137.

Anderson, G., B. Aagaard, and K. Hudnut (2003). Fault interactions and large complex earthquakes in the Los Angeles area, *Science* **302,** 1946–1949.

Arnadottir, T., J. Beavan, and C. Pearson (1995). Deformation associated with the 18 June 1994 Arthur's Pass earthquake, New Zealand, *J. Geol. Geophys.* **38,** 553–558.

Belardinelli, E. M., M. Cocco, O. Coutant, and F. Cotton (1999). Redistribution of dynamic stress during coseismic ruptures: evidence for fault interaction and earthquake triggering, *J. Geophys. Res.* **104,** 14,925–14,945.

Ben-Zion, Y., and P. Malin (1991). San Andreas fault zone head waves near Parkfield, California, *Science*, **251,** 1592–1594.

Bilek, S. L., S. Y. Schwartz, and H. R. DeShon (2003). Control of seafloor roughness on earthquake rupture behavior, *Geology* **31,** 455–458.

Brodsky, E. E., V. Karakostas, and H. Kanamori (2000). A new observation of dynamically triggered regional seismicity: earthquakes in Greece following the August 1999 Izmit, Turkey, earthquake, *Geophys. Res. Lett.* **27,** 2741–2744.

Carena, S., and J. Suppe (2002). Three-dimensional imaging of active structures using earthquake aftershocks: the Northridge thrust, California, *J. Struct. Geol.* **24,** 887–904.

Das, S., and C. H. Scholz (1981). Off-fault aftershock clusters caused by shear stress increase? *Bull. Seism. Soc. Am.* **71,** 1669–1675.

Dorbath, C., D. Oppenheimer, F. Amelung, and G. King (1996). Seismic tomography and deformation modeling of the junction of the San Andreas and Calaveras faults, *J. Geophys. Res.* **101,** 27,017–27,941.

Dreger, D. S., and D. V. Helmberger (1993). Determination of source parameters at regional distances with 3-component sparse network data, *J. Geophys. Res.* **98,** 8107–8125.

Dziewonski, A. M., G. Ekstrom, and M. P. Salganik (1995). Centroid-moment tensor solutions for April–June 1994, *Phys. Earth Planet. Inter.* **88,** 69–78.

Eberhart-Phillips, D., and A. J. Michael (1998). Seismotectonics of the Loma Prieta, California, region determined from three-dimensional V_p, V_p/V_s, and seismicity, *J. Geophys. Res.* **103,** 21,099–21,120.

Felzer, K. R., R. E. Abercrombie, and G. Ekstrom (2003). Secondary aftershocks and their importance for aftershock production, *Bull. Seism. Soc. Am.* **93,** 1443–1448.

Fukuyama, E., W. L. Ellsworth, F. Waldhauser, and A. Kubo (2003). Detailed fault structure of the 2000 western Tottori, Japan, earthquake sequence, *Bull. Seism. Soc. Am.* **93,** 1468–1478.

Garcia, S., J. Angelier, F. Bergerat, and C. Homberg (2002). Tectonic analysis of an oceanic transform fault zone based on fault-slip data and earthquake focal mechanisms: the Husavik-Flatey fault zone, Iceland, *Tectonophysics* **344,** 157–174.

Gerstenberger, M., S. Wiemer, and D. Giardini (2001). A systematic test of the hypothesis that the *b* value varies with depth in California, *Geophys. Res. Lett.* **28,** 57–60.

Gomberg, J. S., and M. A. Ellis (1994). Topography and tectonics of the central New Madrid Seismic zone: results of numerical experiments using a three-dimensional boundary-element program, *J. Geophys. Res.* **99,** 20,299–20,310.

Got, J.-L., J. Fréchet, and F. W. Klein (1994). Deep fault plane geometry inferred from multiplet relative relocation beneath the south flank of Kilauea, *J. Geophys. Res.* **99,** 15,375–15,386.

Hardebeck, J. L., and P. M. Shearer (2002). A new method for determining first-motion focal mechanisms, *Bull. Seism. Soc. Am.* **92,** 2264–2276.

Hardebeck, J. L., and P. M. Shearer (2003). Using *S*/*P* amplitude ratios to constrain the focal mechanisms of small earthquakes, *Bull. Seism. Soc. Am.* **93,** 2434–2444.

Hardebeck, J. L., J. J. Nazareth, and E. Hauksson (1998). The static stress change triggering model: constraints from two southern California aftershocks sequences, *J. Geophys. Res.* **103,** 24,427–24,437.

Harris, R. A. (1998). Introduction to special section: stress triggers, stress shadows, and implications for seismic hazard, *J. Geophys. Res.* **103,** 24,347–24,358.

Harris, R. A., and R. W. Simpson (2002). The 1999 M_w 7.1 Hector Mine, California, earthquake: a test of the stress shadow hypothesis? *Bull. Seism. Soc. Am.* **92,** 1497–1512.

Hessami, K., H. A. Koyi, and C. J. Talbot (2001). The significance of strike-slip faulting in the basement of the Zagros fold and thrust belt, *J. Petrol. Geol.* **24,** 5–28.

Hsu, S. K., and J. C. Sibuet (1995). Is Taiwan the result of arc-continent or arc-arc collision? *Earth Planet. Sci. Lett.* **136,** 315–324.

Igel, H., G. Jahnke, and Y. Ben-Zion (2002). Numerical simulation of fault zone guided waves: accuracy and 3-D effects, *Pure Appl. Geophys.* **159,** 2067–2083.

Imoto, M. A. (2003). Testable model of earthquake probability based on changes in mean event size, *J. Geophys. Res.* **108,** 2082.

Julian, B. R., and G. R. Foulger (1996). Earthquake mechanisms from linear-programming inversion of seismic-wave amplitude ratios, *Bull. Seism. Soc. Am.* **86,** 972–980.

Kagan, Y. Y., (2000). Temporal correlations of earthquake focal mechanisms, *Geophys. J. Int.* **143,** 881–897.

Kilb, D. (2003). A strong correlation between induced peak dynamic Coulomb stress change from the 1992 M 7.3 Landers earthquake and the hypocenter of the 1999 M 7.1 Hector Mine earthquake, *J. Geophys. Res.* **108,** doi 10.1029/2001JB000678.

Kilb, D., and A. M. Rubin (2002). Relocated microearthquakes of the Mt. Lewis M_L 5.7, California, earthquake sequence: implications of diverse fault orientations, *J. Geophys. Res.* **107,** 2294.

Kilb, D., M. Ellis, J. Gomberg, and S. Davis (1997). On the origin of diverse aftershock mechanisms following the 1989 Loma Prieta earthquake, *Geophys. J. Int.* **128,** 557–570.

Kilb, D., J. Gomberg, and P. Bodin (2002). Aftershock triggering by complete colomb stress changes, *J. Geophys. Res.* **107,** doi 10.1029/2001JB000202.

King, G. C. P., and D. D. Bowman (2003). The evolution of regional seismicity between large earthquakes, *J. Geophys. Res.* **108,** 2096.

King, G. C. P., and M. Cocco (2001). Fault interaction by elastic stress changes: new clues from earthquake sequences, *Adv. Geophys.* **44,** 1–38.

King, G. C. P., R. S. Stein, and J. Lin (1994). Static stress changes and the triggering of earthquakes, *Bull. Seism. Soc. Am.* **84,** 935–953.

Kisslinger, C. (1980). Evaluation of *S* to *P* amplitude ratios for determining focal mechanisms from regional network observations, *Bull. Seism. Soc. Am.* **70,** 999–1014.

Lund, B., and R. Boovarsson (2002). Correlation of microearthquake body-wave spectral amplitudes, *Bull. Seism. Soc. Am.* **92,** 2419–2433.

Michelini, A., and A. Lomax (2004). The effect of velocity structure errors on double-difference earthquake location, *Geophys. Res. Lett.* **31,** L09602.

Nadeau, R. M., and T. V. McEvilly (1999). Fault slip rates at depth from recurrence intervals of repeating microearthquakes, *Science* **285,** 718–721.

Nakamura, M. (2002). Determination of focal mechanism solution using initial motion polarity of *P* and *S* waves, *Earth Planet. Inter.* **130,** 17–29.

Oppenheimer, D., F. Klein, J. Eaton, and F. Lester (1993). The Northern California Seismic Network Bulletin January–December 1992, U.S. Department of the Interior, *U.S. Geol. Surv. Open-File Rept. 93-578*.

Oppenheimer, D. H., P. A. Reasenberg, and R. W. Simpson (1988). Fault plane solutions for the 1984 Morgan Hill, California, earthquake sequence: evidence for the state of stress on the Calaveras fault, *J. Geophys. Res.* **93,** 9007–9026.

Reasenberg, P., and D. Oppenheimer (1985). FPFIT, FPPLOT and FPPAGE: FORTRAN computer programs for calculating and displaying earthquake fault-plane solutions, *U.S. Geol. Surv. Open File Rept., 85-739*.

Robinson, D. P., C. Henry, S. Das, and J. H. Woodhouse (2001). Simultaneous rupture along two conjugate planes of the Wharton Basin earthquake, *Science* **292,** 1145–1148.

Robinson, R., M. Reyners, T. Webb, T. Arnadottir, J. Beavan, J. Cousins, R. VanDissen, and C. Pearson (1995). The M_w 6.7 Arthur's Pass earthquake in Southern Alps, New Zealand, June 18, 1994, *Seism. Res. Lett.* **66,** 11–12.

Rockwell, T. K., S. Lindvall, T. Dawson, R. Langridge, W. Lettis, and Y. Klinger (2002). Lateral offsets on surveyed cultural features resulting from the 1999 Izmit and Duzce earthquakes, Turkey, *Bull. Seism. Soc. Am.* **92,** 79–94.

Roumelioti, Z., A. Kiratzi, and N. Melis (2003). Relocation of the 26 July 2001 Skyros Island (Greece) earthquake sequence using the double-difference technique, *Phys. Earth Planet. Inter.* **138,** 231–239.

Rowe, C. A., R. C. Aster, W. S. Phillips, R. H. Jones, B. Borchers, and M. C. Fehler (2002). Using Automated, high-precision repicking to improve delineation of microseismic structures at the Soultz Geothermal Reservoir, *Pure Appl. Geophys.* **159,** 563–596.

Rubin, A. M. (2002a). Using repeating earthquakes to correct high-precision earthquake catalogs for time-dependent station delays, *Bull. Seism. Soc. Am.* **92,** 1647–1659.

Rubin, A. M. (2002b). Aftershocks of microearthquakes as probes of the mechanics of rupture, *J. Geophys. Res.* **107,** 2142, doi 10.1029/2001JB000496.

Rubin, A. M., and D. Gillard (2000). Aftershock asymmetry/rupture directivity along the central San Andreas fault, *J. Geophys. Res.* **105,** 19,095–19,109.

Rubin, A. M., D. Gillard, and J.-L. Got (1999). Streaks of microearthquakes along creeping faults, *Nature* **400,** 635–641.

Rundquist, D. V., and P. O. Sobolev (2002). Seismicity of midoceanic ridges and its geodynamic implications: a review. *Earth-Sci. Rev.* **58,** 143–161.

Scarfi, L., H. Langer, and G. Stefano (2003). High-precision relative locations of two microearthquake clusters in southeastern Sicily, Italy, *Bull. Seism. Soc. Am.* **93,** 1479–1497.

Schaff, D. P., H. R. Gotz, and G. C. Beroza (2002). High-resolution image of Calaveras fault seismicity, *J. Geophys. Res.* **107,** 186.

Segall, P. (2002). Integrating geologic and geodetic estimates of slip rate on the San Andreas fault system, *Int. Geol. Rev.* **44,** 62–82.

Shearer, P. M. (2002). Parallel fault strands at 9-km depth resolved on the Imperial Fault, southern California, *Geophys. Res. Lett.* **29,** doi 10.1029/2002GL015302.

Shearer, P. M., J. L. Hardebeck, L. Astiz, and K. B. Richards-Dinger (2003). Analysis of similar event clusters in aftershocks of the 1994 Northridge, California, earthquake, *J. Geophys. Res.* **108,** B1, doi 10.1029/2001JB000685.

Steacy, S., J. Gomberg, and M. Cocco (2005). Introduction to special section: stress transfer, earthquake triggering, and time-dependent seismic hazard, *J. Geophys. Res.* **110,** B05S01.

Stein, R. S. (1999). The role of stress transfer in earthquake occurrence, *Nature* **402,** 605–609.

Tibi, R., D. A. Wiens, and I. Hiroshi (2003). Remote triggering of deep earthquakes in the 2002 Tonga sequences, *Nature* **424,** 921–925.

Toda, S., and R. Stein (2003). Toggling of seismicity by the 1997 Kagoshima earthquake couplet: a demonstration of time-dependent stress transfer, *J. Geophys. Res.* **108,** 2567.

Toda, S., R. S. Stein, P. A. Reasenberg, J. H. Dieterich, and A. Yoshida (1998). Stress transferred by the 1995 M_w 6.9 Kobe, Japan, shock: effect on aftershocks and future earthquake probabilities, *J. Geophys. Res.* **103,** 24,543–24,565.

Waldhauser, F., and W. L. Ellsworth (2002). Fault structure and mechanics of the Hayward Fault, California, from double-difference earthquake locations, *J. Geophys. Res.* **107,** 2054.

Waldhauser, F., W. L. Ellsworth, and A. Cole (1999). Slip-parallel seismic lineations along the northern Hayward fault, California, *Geophys. Res. Lett.* **26,** 3525–3528.

Wiemer, S., and M. Wyss (2002). Mapping spatial variability of the frequency-magnitude distribution of earthquakes, *Adv. Geophys.* **45,** 259–302.

Wolfe, C. J. (2002). On the mathematics of using difference operators to relocate earthquakes, *Bull. Seism. Soc. Am.* **92,** 2879–2892.

Wyss, M., and S. Wiemer (2000). Change in the probability for earthquakes in southern California due to the Landers magnitude 7.3 earthquake, *Science* **290,** 1334–1338.

Cecil H. and Ida M. Green Institute of Geophysics and Planetary Physics
IGPP/University of California, San Diego
La Jolla, California 92093
(D.K.)

U.S. Geological Survey
345 Middlefield Rd.
Menlo Park, California 94025
(J.L.H.)

Manuscript received 15 December 2004.